

High-trans fatty acid and high-sugar diets can cause mice with non-alcoholic steatohepatitis with liver fibrosis and potential pathogenesis

Xin Xin

Shuguang Hospital

Bei-yu Cai

Shuguang Hospital

Cheng Chen

Shuguang Hospital

Hua-jie Tian

Shuguang Hospital

Xin Wang

Shuguang Hospital

Yi-Yang Hu

Shuguang Hospital

Feng Qin (✉ fengqin1227@163.com)

Shuguang Hospital <https://orcid.org/0000-0002-4641-1636>

Research

Keywords: NASH, Fibrosis, Animal model, Pathogenesis

Posted Date: January 22nd, 2020

DOI: <https://doi.org/10.21203/rs.2.21575/v1>

License:   This work is licensed under a Creative Commons Attribution 4.0 International License.

[Read Full License](#)

Abstract

Aims To establish a mouse model of non-alcoholic steatohepatitis (NASH) within liver fibrosis using a high-fat and high-carbohydrate diet (HFHC) and to analyze potential pathogenesis using a transcriptome microarray.

Methods Sixty mice were stratified by weight and randomly divided into HFHC model and control (Con) groups, with 30 mice in each group. Both HFHC and Con mice were euthanized at 0, 20 and 30 weeks. The following analyses were performed: biochemical analysis; histological assessment; Col-I, α -SMA and TGF- β 1 protein and mRNA expression levels; and transcriptomic gene chip analysis.

Results Compared with the Con group at each time point, the body weight and liver wet weight of the HFHC model group mice were significantly higher. At 30 weeks, ALT, AST, FBG and FINS levels or activities and TG and HYP contents in the HFHC model group were significantly elevated. Severe steatosis was present in the liver tissues from HFHC group mice. Substantial perisinusoidal fibrosis with a cage-like structure and bridging formations were observed in the liver. Col-I, α -SMA and TGF- β 1 protein and mRNA expression levels in liver tissues from HFHC mice increased over time. Compared with the Con group, the HFHC group had 151 differentially expressed genes that were involved in 41 signaling pathways.

Conclusions After 30 weeks of a HFHC diet, the mice exhibited substantial liver fibrosis, hepatic steatosis, ballooning degeneration and inflammation. The formation of an experimental NASH combined with liver fibrosis mouse model may be related to ECM-receptor interaction, Toll-like receptor signaling and other signaling pathways.

Key Points

1. The incidence of fibrotic diseases is high, and there are no ideal therapeutic drugs or an ideal animal model for the drug development process.
2. By feeding mice a high-fat and high-sugar diet for 30 weeks, a non-alcoholic fatty hepatitis fibrosis mouse model can be successfully established.
3. The liver of this model mouse was genetically analyzed and screened to predict possible pathogenesis.

1. Introduction

Non-alcoholic fatty liver disease (NAFLD) has become a common chronic liver disease worldwide. The disease spectrum of NAFLD includes non-alcoholic simple fatty liver (NAFL), non-alcoholic steatohepatitis (NASH), fatty liver fibrosis and liver cirrhosis.¹ Previous studies have shown that liver fibrosis is the most important predictive indicator affecting NAFLD prognosis, and fibrotic staging is closely associated with long-term total mortality, liver transplant and liver-related events.²

Animal models play important roles in investigating disease pathogenesis, assessing diagnostic methods, and screening for effective preventive and treatment drugs. Establishment of appropriate animal models is important for understanding the pathogenesis of liver fibrosis in patients with NAFLD, assessing drug efficacy, and investigating the pharmacological mechanisms. Ideal animal models would not only recapitulate the pathological changes in liver fibrosis in human NASH but also have other disease symptoms of metabolic syndrome, including obesity, hyperlipidemia and insulin resistance, which better simulate the background status of systemic metabolic disorders at human NASH onset. Currently, ideal animal models for fatty liver fibrosis are still rare. A diet rich in saturated fats and fructose is associated with the development of obesity and NASH in humans. A simple high-fat or high-carbohydrate diet can lead to inflammatory steatosis in the liver tissue of animals but fails to produce significant fibrosis. Kohli et al.³ successfully induced NASH-related liver fibrosis using a combination of a high-fat and high-carbohydrate diet for 16 weeks. However, according to their report, liver fibrosis was present in only 50% of the mice, and all the fibrosis was at the F1 or F2 stage, with none of the mice reaching the F3 or F4 fibrotic stage.³ Because early-stage fatty liver fibrosis was observed in this animal model, this model is not ideal for assessment of the efficacy of anti-liver fibrosis treatments. Liver fibrosis incidence in patients with NAFLD significantly prolongs the disease duration, which is an important risk factor for the onset of liver fibrosis in patients with fatty liver disease. Therefore, based on the study by Kohli et al.,³ this current study extended the high-fat and high-carbohydrate diet duration to 20 and 30 weeks with the same formulations used in the Kohli et al.³ study. We dynamically observed successful liver fibrosis model rates and severities in this model and analyzed pathogenesis using transcriptome microarray analysis to provide an appropriate animal model for future drug efficacy assessments.

Therefore, the aim of this study was to develop a NASH model that generates significant fibrosis in nongenetically modified mice whose obesity was induced by diet.

2. Materials And Methods

2.1 Materials

2.1.1 Animals

Sixty 6-week-old, wild-type, male C57BL/6 SPF mice with a body mass of 20-22 g were purchased from Shanghai SLAC Laboratory Animal Co., Ltd. and kept, modeled and observed in a barrier-protected animal room in the animal research center at Shanghai University of Traditional Chinese Medicine. During model establishment, experimental animals had free access to food and water (SYXK (Shanghai) 2014-0008).

2.1.2 Diet

The diet for the high-fat and high-carbohydrate (HFHC) model group was a 58 kcal% fat w/sucrose Surwit Diet (D12331, Lot number: 17082101A10, Research Diets, USA), and the diet for the control (Con) group was an 11 kcal% fat w/cornstarch Surwit Diet (D12328, Lot number: 17100212A4, Research Diets, USA).

Fructose and sucrose (F0001/S0001) were purchased from Trophic Animal Feed High-Tech Co., Ltd, China.

2.2 Methods

2.2.1 Animal grouping and model establishment

All animal experiment protocols were approved by Animal Experimental Ethics Committee of Shanghai University of Traditional Chinese Medicine. C57Bl/6 mice were housed in the animal research center at Shanghai University of Traditional Chinese Medicine. After one week of acclimation, the mice were randomly divided into the Con group (n=30) and the HFHC model group (n=30) according to their body weights. Mice in the HFHC model group were given free access to a high-fat (58% kcal fat, 25% kcal carbohydrate and 17% kcal protein) and high-carbohydrate (drinking water: 42 g/L, 55% fructose and 45% sucrose) diet, and the mice were equally divided at 0 (HFHC 0w), 20 (HFHC 20w) and 30 weeks (HFHC 30w), with 10 mice included at each time point. The Con group mice were fed a corresponding low-fat diet (10.5% fat, 73.1% kcal carbohydrate and 16.4% kcal protein) and normal drinking water; these mice were also equally divided at 0 (Con 0w), 20 (Con 20w) and 30 weeks (Con 30w), with 10 mice included at each time point.

2.2.2 Specimen collection

At the end of weeks 0, 20 and 30, mice were fasted for 12 h and anesthetized with 2% pentobarbital sodium at a dose of 3 mL/kg via intraperitoneal injection. Eyeballs were removed, and 1 mL of blood was collected from each mouse. A piece of liver tissue was extracted from the same lobe and position in each mouse and fixed in 10% neutral buffered formalin solution.

2.2.3 Biochemical analysis

▣ Hepatic enzymatic changes: Serum alanine aminotransferase (ALT) and serum aspartate aminotransferase (AST) were measured using ALT and AST assay kits (Lot number 20180628, Nanjing Jiancheng Bioengineering Institute, Nanjing, China). ▣ Glucose metabolism: Following 12 h of fasting, approximately 3 μ l of blood was collected from the tail vein, and fasting blood glucose (FBG) was measured with a Roche blood glucose meter (Roche diagnostic GmbH, Germany). Fasting insulin (FINS) levels in the serum of mice from each group were measured with an enzyme-linked immunosorbent assay (ELISA) kit (Ultra Sensitive Mouse Insulin ELISA Kit, lot number: 90080, Crystal Chem, USA). The homeostatic model assessment-insulin resistance (HOMA-IR) index was calculated with the following formula: $\text{FBG (mM)} \times \text{FIN (IU/L)} / 22.5$. ▣ Liver triglyceride (TG) content was measured with a kit (Lot number: 2018080029, Dong'ou Diagnostic Products Co. Ltd., Zhejiang, China). ▣ Liver hydroxyproline (HYP) content was measured with a HYP assay kit (Lot number: 20180630, Nanjing Jiancheng Bioengineering Institute, Nanjing, China).

2.2.4 Hematoxylin and eosin (HE) and Sirius red staining

Fixed liver tissue was dehydrated and embedded using a tissue processor (Leica ASP300) and paraffin embedding station (Leica EG1160). Then, sections were then stained using an HE staining kit (Lot number 20180530, Nanjing Jiancheng Bioengineering) and a Sirius red staining kit (Lot number 20180528, Nanjing Jiancheng Bioengineering).

2.2.5 Oil red O staining

Liver tissue was fixed in liquid nitrogen, embedded in ornithine carbamoyl transferase (OCT) medium and sectioned at -20°C at a thickness of 10 µm. The sections were stained using an oil red O staining kit (Lot number 20180528, Nanjing Jiancheng Bioengineering).

2.2.6 Western blot analysis

Antibodies targeting the following proteins were used in this study: α-smooth muscle actin (α-SMA, ab5694, 1:1,000), hepatic type I collagen (Col-I, ab34710, 1:1,000), and transforming growth factor-β1 (TGF-β1, Abcam, 1:1,000). Glyceraldehyde-3-phosphate dehydrogenase (GAPDH) protein expression was used as an internal control.

2.2.7 Immunohistochemistry (IHC)

Samples were first incubated in anti-α-SMA antibody at a dilution of 1:100 (α-SMA, 1:100, catalog number: ab5694, USA) overnight at 4°C and then incubated with primary antibody at a dilution of 1:250. Some liver sections were also stained with anti-Col-I antibody (Col-I, Abcam, 1:100, ab34710, USA) using the same method.

2.2.8 Reverse transcription polymerase chain reaction (RT-PCR)

RNA extraction: RNA was extracted using a UNIQ-10 pillar Trizol total RNA extraction kit (Catalog number: E928KA9723, Sangon Biotech, Shanghai). The relative quantity (RQ) values of the PCR products were subjected to analysis using the $\Delta\Delta$ CT method to assess the messenger RNA (mRNA) expression levels of Col-1, α-SMA, TGF-β1, Col-4 and Smad3.

2.2.9 Library preparation and Illumina Hiseq xten sequencing

Libraries were size selected for cDNA target fragments of 200–300 bp on 2% Low Range Ultra Agarose, followed by PCR amplification using Phusion DNA polymerase (NEB) for 15 PCR cycles. After quantification with a TBS380 fluorometer, the paired-end RNA-seq sequencing library was sequenced with an Illumina HiSeq xten sequencing system (2 × 150 bp read length).

The data were analyzed using the free online Majorbio I-Sanger Cloud Platform (www.i-sanger.com).

2.2.10 Statistical analysis

Statistical analysis of database data was performed using SPSS22.0 software for Mac OS. The measurement data in the statistical description are indicated by S and refer to the count data. When the normality and homogeneity of the variance were satisfied, a t test was applied for comparison of the two groups. The comparison of the hierarchical grouping data was calculated via Radit analysis.

3. Results

3.1 Changes in food and water intake, body mass and liver wet weight levels between each group

3.1.1 Liver appearance in mice from each group

Grossly, the livers in the Con group were dark red and soft. The livers in the HFHC group showed different degrees of yellow at different time points and looked full and blunt; the sections were greasy, and the texture became tough. At 30 weeks, some HFHC mice had yellowish white focal fat deposition in their livers (Fig. 1A).

3.1.2 Changes in average food intake, water intake and liver wet weight

No mice died during the experiment. The body mass of the mice in each group increased gradually over time (Fig. 1B). At 20 weeks, the body mass and liver wet weight in the HFHC group were significantly increased ($P < 0.01$). Compared with those of the Con group mice at 30w, the body mass and liver wet weight levels of the HFHC group mice at 30w were significantly higher ($P < 0.01$). Compared with those the HFHC group mice at 20w, the body mass and liver wet weight levels of the HFHC group mice at 30w were significantly higher ($P < 0.05$, $P < 0.05$) (Fig. 1C). The average food and water intake levels gradually increased over time, with no significant differences observed between the HFHC and Con groups at each time point ($P > 0.05$) (Fig. 1D-F).

3.2 Enzymology and glucose metabolism status in each group

3.2.1 Changes in ALT and AST activities in each group

At 20 weeks, the serum ALT and AST activities in the HFHC group mice were significantly elevated ($P < 0.01$), and these activities increased progressively over time. At 30 weeks, the serum ALT and AST activities in the HFHC group mice were significantly higher than those in the Con group mice ($P < 0.01$) at 30w and the HFHC group mice at 20w ($P < 0.01$, $P < 0.01$) (Fig. 2A and B).

3.2.2 Changes in FBG, FINS and HOMA-IR in each group

Compared with the Con group mice at 20w, the FBG and FINS levels in the HFHC group mice at 20w were significantly higher ($P<0.05$, $P<0.01$), and these levels increased progressively over time. At 30 weeks, the FBG and FINS levels in the HFHC group mice were elevated even more compared with those in Con group mice ($P<0.05$, $P<0.01$). Compared with the Con group mice at the same time points, the HOMA-IR indices in the HFHC group mice were significantly higher ($P<0.01$, $P<0.05$). (Fig. 2C-E).

3.3 Liver steatosis and inflammation status of the mice in each group

3.3.1 Changes in liver TG content

The TG liver content increased gradually over time in both mouse groups. At 20 weeks, the TG liver content in the HFHC group was significantly elevated compared with that in the Con group ($P<0.01$). Similarly, at 30 weeks, the TG liver content in the HFHC group was significantly elevated compared with that in the Con group ($P<0.01$). Additionally, the TG content in the HFHC group at 30w was significantly higher than that at 20w ($P<0.05$) (Fig. 3C).

3.3.2 HE staining

Under a light microscope, HE staining of the liver tissue showed that hepatic steatosis affected the entire liver lobule, with substantial inflammatory cell infiltration and scattered necrosis. The HFHC mice at 30w showed ballooning degeneration of hepatocytes and inflammatory foci in the hepatic lobule. The NAFLD activity scores (NAS) ranged from 4–8, among which 80% were higher than 5, meeting the NASH diagnosis criteria, and 40% were close to 8 (Fig. 3A and D).

3.3.3 Oil red O staining

The staining showed that both macrovesicular and microvesicular steatosis were present in the liver tissues from mice in the HFHC group at 20w, ranging from 33 to 66%. The area, density and intensity of oil red O staining in liver tissue from the HFHC group increased gradually over time. At 30 weeks, severe macrovesicular and microvesicular steatosis was present in the liver tissues from the HFHC group, ranging from 66 to 99% (Fig. 3B).

3.4 Collagen deposition and hepatic stellate cell (HSC) activation status in liver tissue from mice in each group

3.4.1 HYP content

The liver HYP content in the HFHC group increased gradually over time. Compared with that in the Con group at 20w, the liver HYP content in the HFHC group mice at 20w was significantly increased ($P < 0.05$). Similarly, the liver HYP content in the HFHC group at 30w was significantly elevated compared with that in the Con group at 30w ($P < 0.01$) and the HFHC group at 20w ($P < 0.05$) (Fig. 4A).

3.4.2 Sirius red staining

Under a light microscope, Sirius red staining of the liver tissue showed that at 20 weeks, fibrosis in the perisinusoidal space was present in a star shape in the HFHC mouse livers, and the fibrosis stage ranged from F1-F2, with the majority (60%) at stage F2. At 30 weeks, there was substantial perisinusoidal fibrosis in the liver, the presence of cage-like structures, and massive fibrous connective tissue hyperplasia, with some bridging formations. Semiquantitative analysis showed that at 30 weeks, the collagen level in the HFHC group was significantly higher than that in the Con group ($P < 0.01$), and more than half of the fibrosis was at the F2-F3 stage (Fig. 4B-D).

3.4.3 Changes in the Col-I, α -SMA and TGF- β 1 protein expression levels in liver tissues from mice in each group

Western blot analysis showed that the Col-I, α -SMA and TGF- β 1 protein expression levels in the HFHC group livers at 20w and 30w were significantly higher than those in Con group livers at 0w, and the expression levels increased over time ($P < 0.01$, $P < 0.01$, $P < 0.05$) (Fig. 5A).

3.4.4 IHC of Col-1 and α -SMA in the mouse livers in each group

This α -SMA-positive staining was significantly enhanced in the fibrotic liver septum in the HFHC group at 20w and 30w and was mainly located in the thick and dense fibrotic septum. The positive staining area increased over time. Similarly, Col-I positive staining was present only in the blood vessel walls in the Con group at 0w. This Col-I positive staining was significantly enhanced in the fibrotic liver septum in the HFHC group at 20w and 30w and was mainly located in the perisinusoidal hepatocyte membranes and fibrotic septum. The positive staining area increased over time (Fig. 5B).

3.4.5 Col-I, Col-4, α -SMA, TGF- β 1, and Smad3 mRNA expression levels in mice in each group

Compared with those in the Con group livers at 0w, the Col-I, TGF- β 1 and α -SMA mRNA expression levels in the HFHC group livers at 20w were significantly increased ($P < 0.05$, $P < 0.05$ and $P < 0.01$). At 30 weeks, the Col-I, Col-4, α -SMA, and TGF- β 1 mRNA levels in the HFHC group livers were significantly increased

($P < 0.01$), and there was a trend toward increased Smad3 mRNA levels, although the difference was not statistically significant (Fig. 5C-G).

3.5 Transcriptome analysis of differential gene expression between the HFHC group and Con group

3.5.1 Model group and normal group differential gene clustering analysis heat map

The genes differentially expressed between the normal group and model group were selected ($P < 0.05$), and a heat map analysis was performed via cluster analysis, as shown in the following figure. The three samples in the normal group and the model group were naturally clustered, and the expression levels of the genes were similar, but the gene expression difference between the two groups was significant (Fig. 6A).

3.5.2 Differentially expressed genes between the model group and normal group

There were 151 differentially expressed genes with different logarithmic values of $\text{Log}_2\text{FC} \geq 2$ and $P < 0.05$ between the model group and the normal group, including 104 upregulated genes (Table.1) and 47 downregulated genes (Table.2).

3.5.3 Signal-regulated pathways associated with the genes differentially expressed between the model group and the normal group

The 151 differentially expressed genes between the model group and the normal group with a fold change ≥ 2 according to Log_2FC values were analyzed via KEGG PATHWAY analysis using R script. When the corrected P value (P_{adjust}) was < 0.05 , the KEGG PATHWAY function was considered to show significant enrichment. The results showed that the above 151 differentially expressed genes were involved in 41 signaling pathways, suggesting that the 41 signaling pathways are significant in the high-trans fatty acid, high-glucose diet-induced NAFLD model (Fig. 6B, Table. 3).

4. Discussion

NAFLD has become a common chronic liver disease worldwide, and its disease spectrum includes NAFL, NASH, fatty liver fibrosis and liver cirrhosis. Currently, NAFLD affects 30% of the population in western countries and 15–40% in China. More than 50% of obese individuals have NAFLD, and 30–42% of

severely obese NASH patients have significant liver fibrosis.¹ A recent study showed that persistent liver injury in approximately 40% of NASH patients progresses to liver fibrosis and liver cirrhosis. Within a decade, the large population of NASH patients could inevitably lead to a high incidence of fatty liver fibrosis and liver cirrhosis. Long-term follow-up studies have shown that liver fibrosis is the most important predictive indicator affecting NAFLD prognosis.^{5,6}

Selection of appropriate animal models is critical for investigations into the pathogenesis of fatty liver fibrosis and for drug development.⁷ Ideal animal models not only recapitulate the pathological changes associated with liver fibrosis in human NASH but also have other metabolic syndrome disease symptoms, including obesity, hyperlipidemia and insulin resistance, which better simulates the background status of systemic metabolic disorders present at the onset of human NASH. Significant progress has been made in the establishment of NAFLD animal models, and in recent years, simple fatty liver animal models have been successfully established. However, currently, ideal animal models for fatty liver fibrosis are still rare. At present, animal models used to study NAFLD primarily include gene knockout/mutation models; animal models induced by chemical toxins, drugs or nutrition deficiency; high-fat diet models; and composite models. Animal models established through genetic mutations or deletions have impaired fatty acid metabolism, leading to spontaneous fatty liver formation accompanied by relevant metabolic syndrome symptoms, including obesity and insulin resistance, which may easily result in hepatocellular carcinoma (HCC). However, many genetic models do not lead to NASH or the natural progression of fibrosis. As a result, those genetic models are only appropriate for investigation of specific NAFLD pathogenesises.⁸ Among the chemical toxin or drug-induced animal models, the CCl₄-induced model was the earliest developed and is the most widely used; this model is characterized by a short induction duration, with easy establishment of significant pathology. However, the biggest limitation of the CCl₄-induced model is that the animals do not become obese or insulin resistant, which differs greatly from the pathophysiological characteristics of human NAFLD.⁹ The animal model induced by a methionine-choline-deficient (MCD) diet shows the typical NASH histological changes but is accompanied by weight loss and a lack of metabolic syndrome.¹⁰

Dietary factors are important environmental factors that cause fatty liver disease. A diet rich in saturated fat and fructose is associated with the development of obesity and NASH in humans. Feeding animals a high-fat or high-carbohydrate diet can successfully induce inflammation and steatosis but fails to generate significant fibrosis. High-fat, high-carbohydrate diets may lead to significant liver fibrosis, inflammation, endoplasmic reticulum stress and apoptosis in fat cells in humans and animals.¹¹ Trans fatty acids (TFAs) are unsaturated fatty acids that contain trans double bonds. Multiple clinical studies have confirmed that excessive TFA consumption increases the probability of developing NASH and that TFA intake reduces the sensitivity of fat cells to insulin, which in turn increases the need for insulin and the pancreatic load and is closely associated with the incidence of type II diabetes in obese individuals.¹² Excessive TFA intake has been shown to induce liver steatosis by increasing fatty acid synthesis and inhibiting fatty acid oxidation.¹³ Other studies have shown that feeding LDL receptor knockout mice¹⁴ and PPAR α knockout mice¹⁵ a high-fat diet enriched in TFAs can accelerate NASH induction. Tetri et al.¹⁶

showed that under the circumstances of obesity and insulin resistance, mice fed fructose and TFAs developed NASH at 12 weeks, and the study further showed that TFAs caused liver injury under certain conditions. Additionally, Kondoh et al.¹⁷ showed that the addition of elaidic acid, the main component of partially hydrogenated vegetable oils, to human liver cells activated caspase 3, leading to apoptosis. These studies show that TFAs play a critical role in the progression of NAFLD to NASH combined with liver fibrosis. Currently, some researchers believe that a combination of TFAs and fructose induces oxidative stress and increases TNF α , IL-6, IL-1 β , and collagen-I α expression levels, which explains the roles of TFA and fructose in fibrosis progression. Additionally, fructose metabolism leads to glyoxal formation and increases reactive oxygen species levels, which induces mitochondrial damage in liver cells. Fructose is also involved in liver steatosis and liver disease progression by promoting lipid synthesis, leptin resistance and the generation of long-lasting endotoxins.¹¹ However, in animal experiments, a simple high-fructose diet is insufficient to induce liver inflammation and fibrosis, and this diet reduces water intake in mice. A combination of fructose and sucrose ensures normal water intake in experimental animals. Therefore, we fed mice a high-fat (especially TFAs) diet and an excessive amount of fructose and sucrose according to a study published in "Hepatology".³ Based on that study, we set different time points, extended the model establishment duration to 20 and 30 weeks, and dynamically observed the pathological features of this model, including liver steatosis, inflammation and collagen deposition. Thus, we established an ideal model that better recapitulates NASH in combination with liver fibrosis and that can be used for drug efficacy assessments.

Our study showed that following 30 weeks of a high-fat (saturated fat + TFAs) and high-carbohydrate (fructose + sucrose) diet the mice were fat and sluggish. Compared with the control group over the same time, the mice in the HFHC model group did not differ significantly in the amount of food and water intake. The body mass of the HFHC group mice at 30w was increased by approximately 100% compared with that of the Con group mice at 30w and 20% compared to that of the HFHC group mice at 20w. The HYP content in the HFHC group was higher than that in the Con group at the same time points. Liver pathological analysis showed that at 20 weeks, macrovesicular and microvesicular steatosis was present in the liver tissues from the HFHC group, ranging from 33 to 66%; inflammatory foci started to appear in the hepatic lobule; fibrosis in the perisinusoidal space was distributed in a star shape; and fibrosis staging ranged from F1-2, with the majority (60%) being at stage F2. At 20 weeks, 80% of the HFHC mice met the pathological diagnostic criteria for NASH, which was accompanied by perisinusoidal fibrosis. Compared with the HFHC group at 20w, the liver tissues from the HFHC group at 30w showed more severe fibrosis and fat deposition, with the presence of severe macrovesicular and microvesicular steatosis, ranging from 66 to 99%, which was accompanied by ballooning degeneration of hepatocytes and inflammatory foci in the hepatic lobule. Compared with the Con group, the liver pathological scores of mice in the HFHC group at 30w were significantly elevated. Sirius red staining showed substantial perisinusoidal fibrosis, the presence of cage-like fibrotic changes, and bridging formations in some of the fibrotic tissue. Semiquantitative analysis showed significantly higher collagen levels in the HFHC group at 30w compared with those in the Con group at 30w. More than 70% of the fibrosis was at stages F2-F3. α -SMA, Col-I and TGF- β 1 protein expression levels in the livers of the HFHC mice at 20w were significantly

higher than those in the livers of the Con group mice at 20w. Consistent with these findings, the α -SMA, Col-I and TGF- β 1 mRNA levels were significantly increased, and significant increases in α -SMA-positive and Col-I-positive staining were observed following 20 weeks of a HFHC diet, which is indicative of HSC activation and collagen deposition in the liver. α -SMA, Col-I and TGF- β 1 protein and mRNA levels increased significantly in the livers of the HFHC mice at 30w compared with those in the livers of the HFHC mice at 20w. α -SMA- and Col-I-positive staining areas in the livers of the HFHC mice at 30w were significantly increased compared with those in the livers of the HFHC mice at 20w. At 30 weeks, the HFHC mice exhibited elevated serum ALT, AST and TG contents, which was accompanied by disrupted glucose metabolism—consistent with natural NASH progression. The HFHC mice at 30w also exhibited major symptoms of metabolic syndrome, indicating that this extended HFHC induction method successfully establishes an animal model for liver fibrosis within NAFLD.

Based on the successful construction of a mouse model of NASH with liver fibrosis that can simulate human pathogenesis and symptoms, in order to better reveal the pathogenic mechanism of the model, we conducted Experiment 2 and compared the control group with the model group. Analysis of transcriptomics chips was performed to facilitate precise identification of pathogenesis mechanisms that can aid in drug development for this disease and improve the success rate and efficiency of new drug development. Through analysis, we found 151 genes with Log₂FC difference multiples greater than 2 and $P < 0.05$ in the high-fat and high-sugar diet group compared with the normal group and used the R script to perform KEGG PATHWAY enrichment analysis of the genes/transcripts in the gene set. A corrected P value < 0.05 was considered to indicate significant enrichment of the KEGG PATHWAY function. The results showed that the above 151 differentially expressed genes were involved in 41 signaling pathways, suggesting that these 41 signaling pathways are significant in the mouse NASH-induced liver fibrosis model. Based on their roles and pathophysiological significance, the 41 signaling pathways associated with these 151 differentially expressed genes revealed in the gene expression analysis likely play a role in the pathological characteristics and related pathogenesis of liver fibrosis induced by nonalcoholic fatty liver in mice.

The results of this transcriptome analysis in the 30-week mice that were fed a high-trans fatty acid and high-sugar water diet revealed significant changes in the expression of 151 genes involved in 41 pathways. Thus, the ECM-receptor interaction pathway, the Toll-like receptor signaling pathway, cytokine-cytokine receptor interaction, the retinol metabolism pathway, steroid hormone biosynthesis, arachidonic acid metabolism, the chemokine signaling pathway, steroid biosynthesis, linoleum/linoleic acid metabolism, the adenosine 5'-monophosphate (AMP) signaling (AMPK signaling) pathway, the peroxisome proliferator-activated receptor signaling (PPAR signaling) pathway, fatty acid degradation, and regulation of lipolysis in adipocytes are highly correlated with the development of NAFLD. Among them, liver fibrosis-related signaling pathways are particularly prominent.

In summary, the mouse model of NASH and liver fibrosis described herein, which was induced by 30 weeks of a high-fat (saturated fat + TFAs) and high-carbohydrate (fructose + sucrose) diet, closely mimics human NASH associated with liver fibrosis and aspects of human biochemistry and pathology.

The high incidence of these pathological changes, high success rate of model establishment and zero mortality rate make this model appropriate for investigating the underlying mechanisms of liver fibrosis within NAFLD and for drug efficacy assessments.

Declarations

Ethics approval and consent to participate

All applicable international, national, and/or institutional guidelines for the care and use of animals were followed.

Consent for publication

Not applicable

Availability of data and materials

All data generated or analysed during this study are included in this published article.

Competing interests

The authors declare that they have no competing interests

Funding

This research was sponsored by the National Natural Science Foundation of China (No. 81573668 to Q. F, No. 81830119 to Y. H.); The National Science and Technology Major Project 'Key New Drug Creation and Manufacturing Program', China (No.2018ZX09201001-001–002 to Q. F); and Shanghai Science and Technology Innovation Fund (No. 18401933100 to Q. F).

Authors' contributions

XX completed animal husbandry, biochemical experiments, immunological experiments, genetic analysis, etc. of this research, and was a major contributor in writing the manuscript. CBY is responsible for the animal husbandry of this study and the operation of some biochemical tests.

CC partly participated in the design of the research experimental scheme. THJ provided some experimental techniques in this study. WX assisted XX in processing the analysis of some experimental data in this study. HYY was responsible for the design of the experimental protocol and the writing of the experimental part of the study. FQ is responsible for the planning of the overall experimental scheme and

participation in the completion of the final manuscript and most of the experiments in this study. All authors read and approved the final manuscript.

Acknowledgements

Not applicable

References

1. Diehl AM, Day C. Cause, pathogenesis, and treatment of nonalcoholic steatohepatitis. *N Engl J Med* 2017;377:2063–2072.
2. Angulo P, Kleiner DE, Dam-Larsen S, et al. Liver fibrosis, but no other histologic features, is associated with long-term outcomes of patients with nonalcoholic fatty liver disease. *Gastroenterology* 2015;149:389–397.e310.
3. Kohli R, Kirby M, Xanthakos SA, et al. High-fructose, medium chain trans fat diet induces liver fibrosis and elevates plasma coenzyme Q9 in a novel murine model of obesity and nonalcoholic steatohepatitis. *Hepatology* 2010;52:934–944.
4. Peng JH, Hu YY, Cheng Y, et al. Effect of JIANPI HUOXUE decoction on inflammatory cytokine secretion pathway in rat liver with lipopolysaccharide challenge. *World J Gastroenterol* 2008;14:1851–1857.
5. Ekstedt M, Hagstrom H, Nasr P, et al. Fibrosis stage is the strongest predictor for disease-specific mortality in NAFLD after up to 33 years of follow-up. *Hepatology* 2015;61:1547–1554.
6. Hagstrom H, Nasr P, Ekstedt M, et al. Fibrosis stage but not NASH predicts mortality and time to development of severe liver disease in biopsy-proven NAFLD. *J Hepatol* 2017;67:1265–1273.
7. London RM, George J. Pathogenesis of NASH: animal models. *Clin Liver Dis* 2007;11:55–74, viii.
8. Anstee QM, Goldin RD. Mouse models in non-alcoholic fatty liver disease and steatohepatitis research. *Int J Exp Pathol* 2006;87:1–16.
9. Kubota N, Kado S, Kano M, et al. A high-fat diet and multiple administration of carbon tetrachloride induces liver injury and pathological features associated with non-alcoholic steatohepatitis in mice. *Clin Exp Pharmacol Physiol* 2013;40:422–430.
10. George J, Pera N, Phung N, Leclercq I, Hou JY, Farrell G. Lipid peroxidation, stellate cell activation and hepatic fibrogenesis in a rat model of chronic steatohepatitis. *J Hepatol* 2003;39:756–764.
11. Lee O, Bruce WR, Dong Q, Bruce J, Mehta R, O'Brien PJ. Fructose and carbonyl metabolites as endogenous toxins. *Chem Biol Interact* 2009;178:332–339.

12. Jeyapal S, Putcha UK, Mullapudi VS, et al. Chronic consumption of fructose in combination with trans fatty acids but not with saturated fatty acids induces nonalcoholic steatohepatitis with fibrosis in rats. *Eur J Nutr* 2018;57:2171–2187.
13. Obara N, Fukushima K, Ueno Y, et al. Possible involvement and the mechanisms of excess trans-fatty acid consumption in severe NAFLD in mice. *J Hepatol* 2010;53:326–334.
14. Machado RM, Stefano JT, Oliveira CP, et al. Intake of trans fatty acids causes nonalcoholic steatohepatitis and reduces adipose tissue fat content. *J Nutr* 2010;140:1127–1132.
15. Hu X, Tanaka N, Guo R, et al. PPAR α protects against trans-fatty-acid-containing diet-induced steatohepatitis. *J Nutr Biochem* 2017;39:77–85.
16. Tetri LH, Basaranoglu M, Brunt EM, Yerian LM, Neuschwander-Tetri BA. Severe NAFLD with hepatic necroinflammatory changes in mice fed trans fats and a high-fructose corn syrup equivalent. *Am J Physiol Gastrointest Liver Physiol* 2008;295:G987–995.
17. Kondoh Y, Kawada T, Urade R. Activation of caspase 3 in HepG2 cells by elaidic acid (t18:1). *Biochim Biophys Acta* 2007;1771:500–505.

Tables

Table 1 Up-regulated differential genes in model group and normal group with Log₂FC \geq 2 and P <0.05

Gene name	Gene description	Con	HFHC	FC(HFHC/Con)	Log2FC	Padjust	Regulate
		(Mean)	(Mean)		(HFHC/Con)		
Sprr1a	Small Proline-rich Protein 1A	0.00	4.59	431.01	8.75	0.0132	up
Cyp2b10	Cytochrome P450, family 2, subfamily b, polypeptide 10	0.10	25.61	274.92	8.10	0.0163	up
Cidea	Cell death-inducing DNA fragmentation factor, alpha subunit-like effector A	0.22	46.42	217.00	7.76	0.0001	up
Mas1	MAS1 oncogene	0.00	0.57	118.42	6.89	0.0156	up
Xlr4a	X-linked lymphocyte-regulated 4A	0.02	3.93	82.35	6.36	0.0330	up
Chil1	Chitinase-like 1	0.03	1.22	79.61	6.31	0.0043	up
Ttc39aos1	Ttc39a opposite strand RNA 1	0.00	1.46	67.28	6.07	0.0409	up
Cyp2b9	Cytochrome P450, family 2, subfamily b, polypeptide 9	1.56	123.01	62.17	5.96	0.0044	up
Prtn3	Proteinase 3	0.00	0.78	59.71	5.90	0.0444	up
Cyp2b13	Cytochrome P450, family 2, subfamily b, polypeptide 13	0.03	1.66	56.33	5.82	0.0103	up
Cfd	Complement factor D (adipsin)	0.23	12.86	52.08	5.70	0.0015	up
Orm3	Orosomuroid 3	0.27	7.06	25.29	4.66	0.0082	up
Nat8f7	N-acetyltransferase 8 (GCN5-related) family member 7	0.06	2.18	25.21	4.66	0.0184	up
Pls1	Plastin 1 (I-isoform)	0.14	0.69	21.32	4.41	0.0161	up
Ciart	Circadian associated repressor of transcription	0.27	5.84	20.40	4.35	0.0186	up

Table 2 Down-regulated differential genes in model group and normal group with $\text{Log2FC} \leq -2$ and $P < 0.05$

Gene name	Gene description	Con	HFHC	FC(HFHC/Con)	Log2FC	Padjust	Regulate
		(Mean)	(Mean)		(HFHC/Con)		
Adra2a	Adrenergic receptor, alpha 2a	0.47	0.02	0.04	-4.70	0.0240	Down
Serpina1e	Serine (or cysteine) peptidase inhibitor, clade A, member 1E	2355.30	94.32	0.04	-4.51	0.0052	Down
Lepr	Leptin receptor	7.01	0.54	0.06	-4.04	0.0043	Down
Cspg5	Chondroitin sulfate Proteoglycan 5	1.11	0.07	0.06	-3.96	0.0046	Down
Enho	Energy homeostasis associated	13.42	1.12	0.09	-3.52	0.0025	Down
Slc30a3	Solute carrier family 30 (zinc transporter), member 3	0.94	0.08	0.09	-3.49	0.0051	Down
Unc79	Unc-79 homolog (C. Elegans)	1.15	0.14	0.13	-3.00	0.0181	Down
Gtpbp4-Ps1	GTP binding Protein 4, Pseudogene 1	54.76	5.16	0.13	-2.97	0.0083	Down
Pitx3	Paired-like homeodomain transcription factor 3	6.66	0.52	0.14	-2.87	0.0033	Down
Slc13a5	Solute carrier family 13 (sodium-dependent citrate transporter), member 5	1.25	0.20	0.14	-2.86	0.0149	Down
Fam198a	Family with sequence similarity 198, member A	5.43	0.78	0.14	-2.80	0.0052	Down
Pdk4	Pyruvate dehydrogenase kinase, isoenzyme 4	33.33	5.43	0.15	-2.74	0.0041	Down
Asns	Asparagine synthetase	1.17	0.40	0.16	-2.68	0.0161	Down
PPP1r3g	Protein phosphatase 1, regulatory (inhibitor) subunit 3G	2.54	0.41	0.16	-2.66	0.0181	Down
Fst	Follistatin	1.47	0.24	0.17	-2.60	0.0056	Down

Table 3 KEGG signaling pathways identified in genes that are differentially expressed between the model group and normal group.

Pathway id	Description	Ratio_in_study	Ratio_in_pop	Percent	P-value
Map00830	Retinol metabolism	23/665	143/22793	16.08%	1.4977E-08
Map00140	Steroid hormone biosynthesis	22/665	144/22793	15.28%	2.6183E-08
Map05204	Chemical carcinogenesis	23/665	176/22793	13.07%	1.3555E-07
Map00590	Arachidonic acid metabolism	19/665	127/22793	14.96%	2.8598E-07
Map04062	Chemokine signaling pathway	24/665	241/22793	9.96%	8.3868E-06
Map00980	Metabolism of xenobiotics by cytochrome P450	15/665	137/22793	10.95%	0.00035448
Map04750	Inflammatory mediator regulation of TRP channels	16/665	161/22793	9.94%	0.00056316
Map00100	Steroid biosynthesis	6/665	23/22793	26.09%	0.00098829
Map00591	Linoleic acid metabolism	10/665	72/22793	13.89%	0.00099817
Map00062	Fatty acid elongation	7/665	38/22793	18.42%	0.00210167
Map00982	Drug metabolism-cytochrome P450	12/665	119/22793	10.08%	0.00324254
Map04152	AMPK signaling pathway	14/665	160/22793	8.75%	0.00416512
Map03320	PPAR signaling pathway	12/665	127/22793	9.45%	0.00529036
Map00071	Fatty acid degradation	8/665	63/22793	12.70%	0.00646651
Map04923	Regulation of lipolysis in adipocytes	8/665	66/22793	12.12%	0.00846127
Map04145	Phagosome	27/665	474/22793	5.70%	0.00990327
Map01040	Biosynthesis of unsaturated fatty acids	6/665	39/22793	15.38%	0.01027708
Map00520	Amino sugar and nucleotide sugar metabolism	8/665	70/22793	11.43%	0.01099148
Map04512	ECM-receptor interaction	9/665	88/22793	10.23%	0.01163767
Map04650	Natural killer cell mediated cytotoxicity	19/665	302/22793	6.29%	0.01575303
Map04974	Protein digestion and absorption	9/665	97/22793	9.28%	0.01992439
Map04060	Cytokine-cytokine receptor interaction	19/665	311/22793	6.11%	0.02042395
Map04918	Thyroid hormone synthesis	8/665	82/22793	9.76%	0.02369879
Map04931	Insulin resistance	10/665	121/22793	8.26%	0.02475499
Map04930	Type II diabetes mellitus	7/665	69/22793	10.14%	0.03251649
Map04920	Adipocytokine signaling pathway	7/665	72/22793	9.72%	0.0399927
Map04620	Toll-like receptor signaling pathway	9/665	111/22793	8.11%	0.04083019
Map04080	Neuroactive ligand-receptor interaction	19/665	341/22793	5.57%	0.04192223
Map04666	Fc gamma R-mediated phagocytosis	15/665	244/22793	6.15%	0.0422101
Map00900	Terpenoid backbone biosynthesis	5/665	40/22793	12.50%	0.04231822
Map04012	ErbB signaling pathway	9/665	115/22793	7.83%	0.04606007

Figures

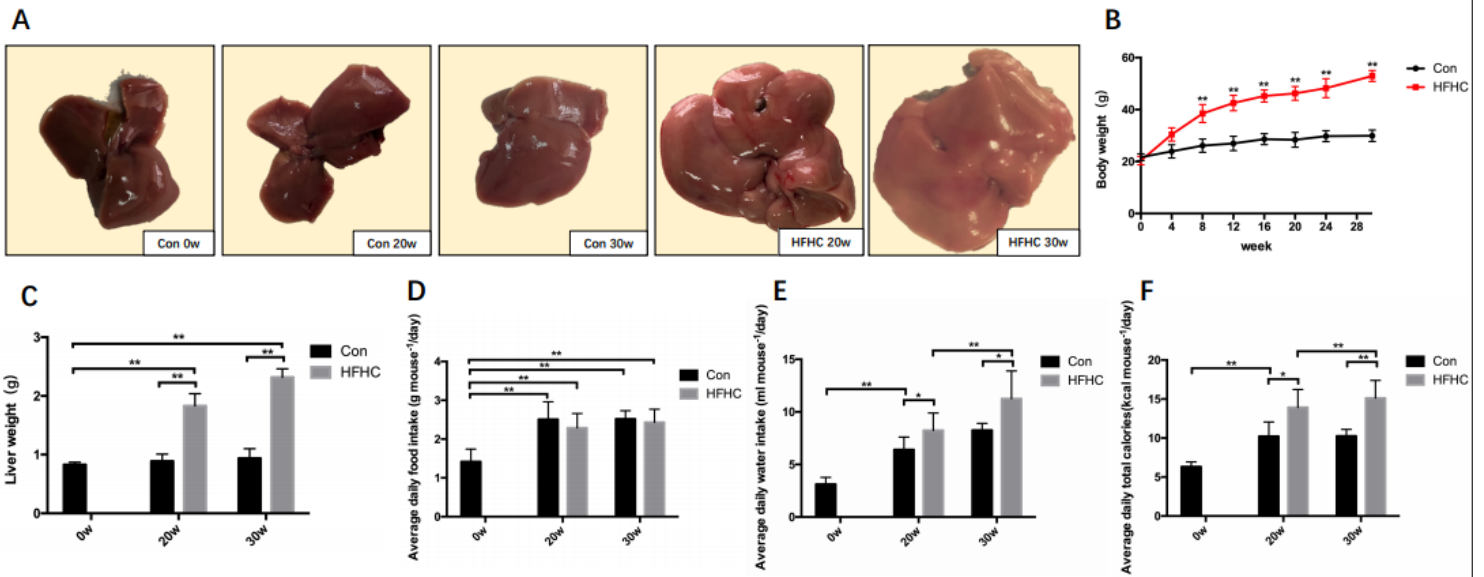


Figure 1

General conditions of the mice in each group A. Changes in liver morphology of mice in each group B. Changes in body weight of mice in each group C. Changes in liver wet weight of mice in each group D-F. Changes in average food intake, water intake and total calories intake of mice in each group When the difference was statistically significant the following symbols were used: *P<0.05, **P<0.01

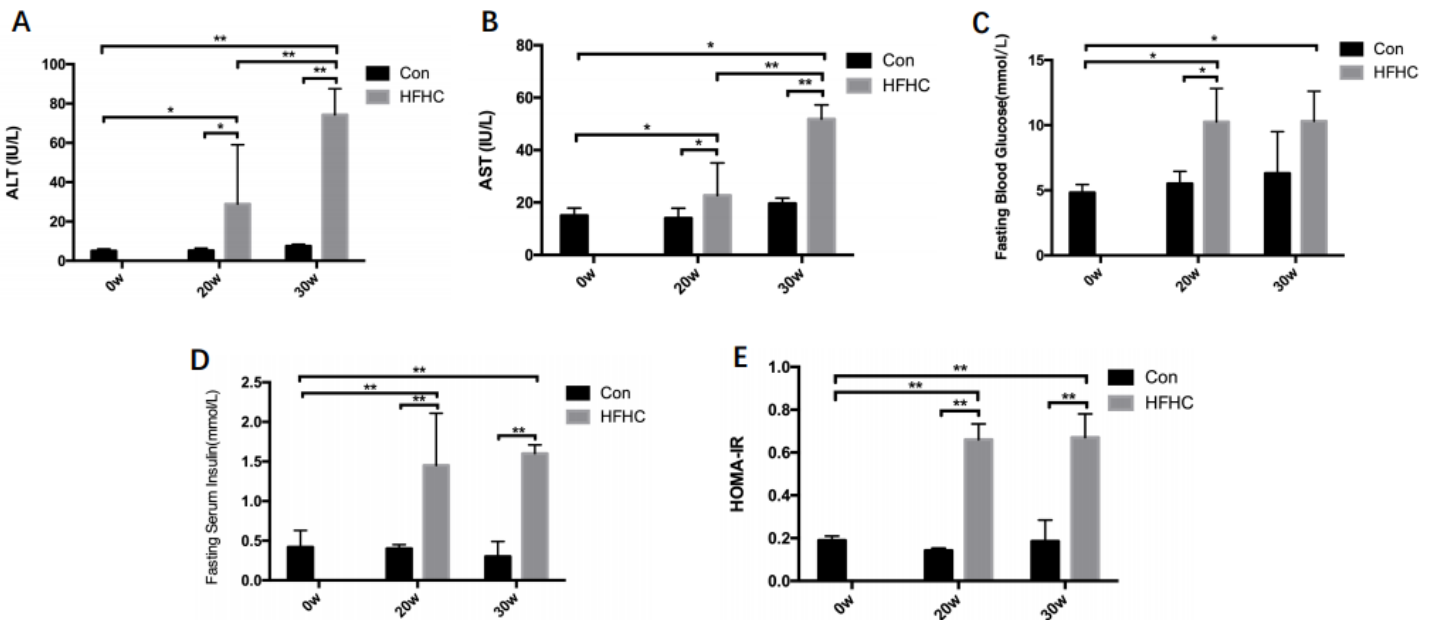


Figure 2

Enzymology and glucose metabolism status of the mice in each group A-E. Changes in serum ALT and AST activities, FBG, FINS and HOMA-IR of the mice from each group When the difference was statistically significant the following symbols were used: *P<0.05, **P<0.01

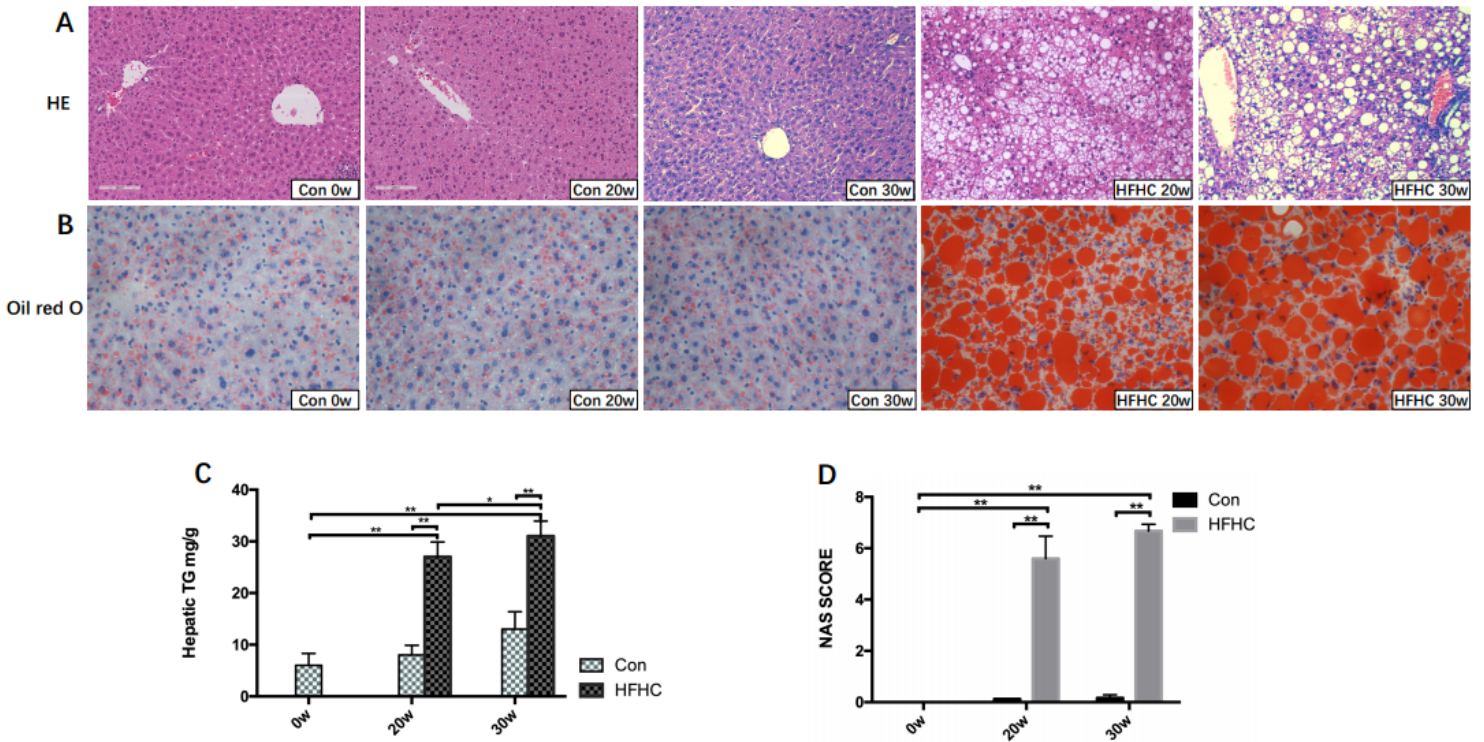
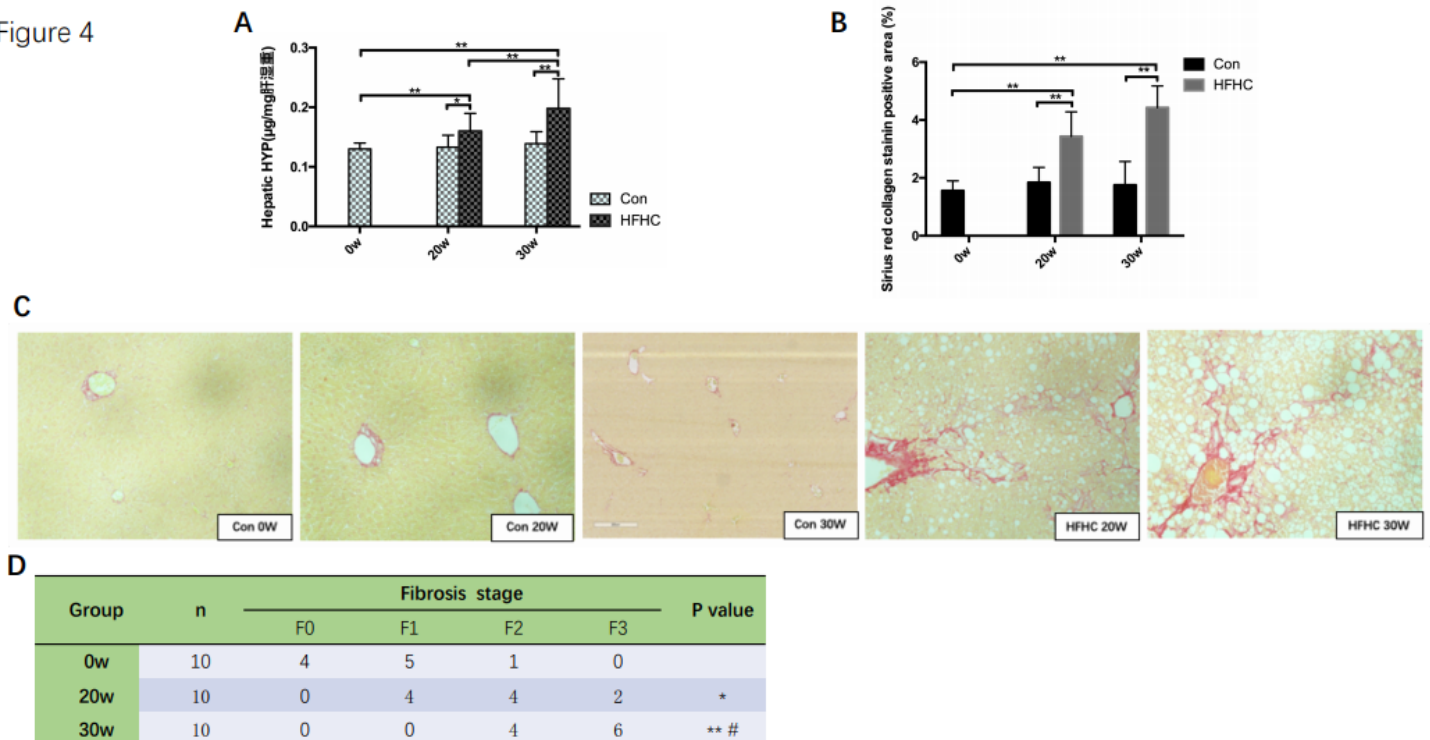


Figure 3

Liver steatosis and inflammation status of the mice in each group A. Liver tissue HE staining (100x). B. Oil red O staining (400x) C. Changes in the liver TG contents of the mice in each group. D. Changes in the NAS SCORE of the mice in each group. When the difference was statistically significant the following symbols were used: *P<0.05, **P<0.01

Figure 4



Note: Compared with the 16w model group, *P<0.05, **P<0.01; compared with the 20w model group, #P<0.05

Figure 4

Collagen deposition in the liver tissue of the mice from each group (Pathology) A. HYP contents B. Liver fibrosis areas with positive collagen levels by semi-quantitative analysis of Sirius red staining C. Sirius red staining (200×) D. Liver fibrosis stage When the difference was statistically significant the following symbols were used: *P<0.05, **P<0.01

Figure 5

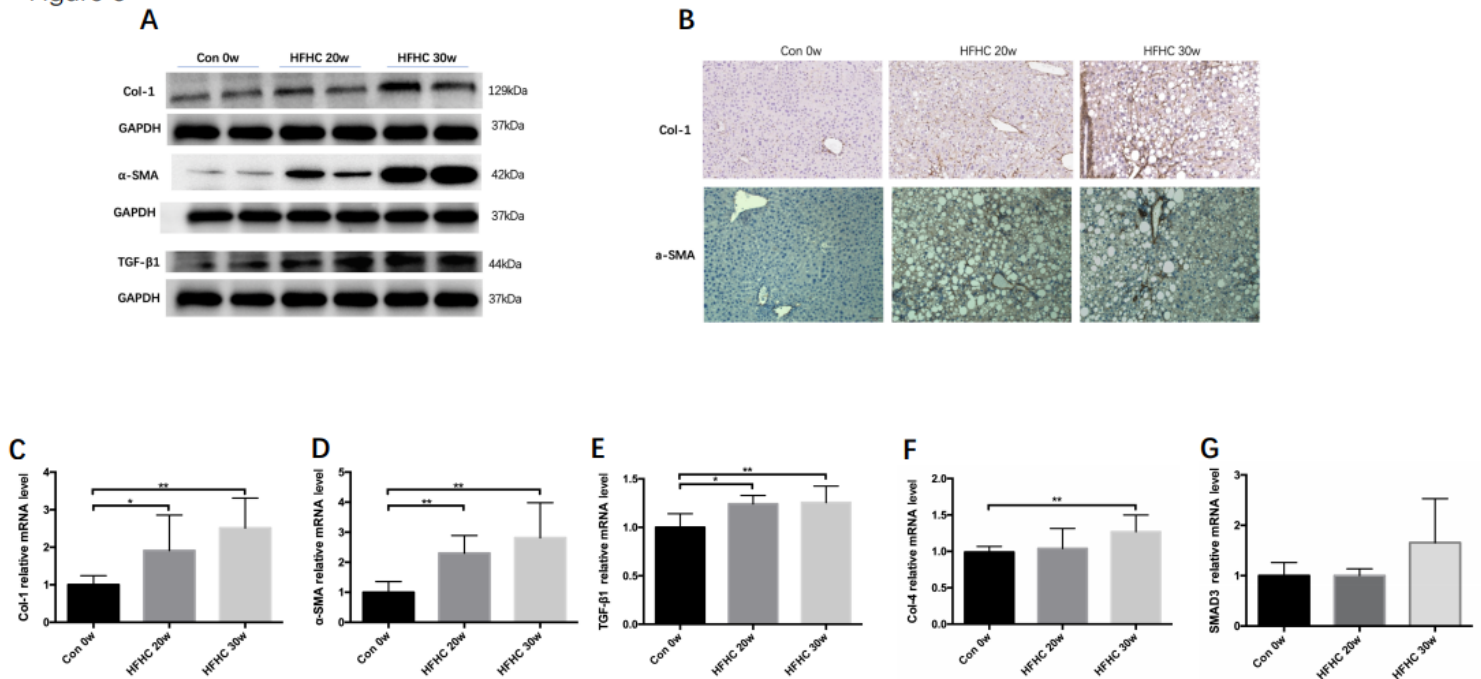


Figure 5

Collagen deposition and HSC activation status in the liver tissue of the mice from each group (Protein and gene expression) A. Col-1, α-SMA and TGF-β1 protein expression levels in liver tissue B. IHC of Col-1 and α-SMA in liver tissue C-G. The mRNA expression levels of Col-1, α-SMA, TGF-β1, Col-4 and Smad3 in liver tissue. When the difference was statistically significant the following symbols were used: *P<0.05, **P<0.01

